# Insights into the significant increase of ozone during COVID-19 in a typical urban city of China

**Kun Zhang [a, b#], Zhiqiang Liu [a, c#], Xiaojuan Zhang [a, c], Qing Li [a, b], Andrew Jensen [d, e], Wen Tan [f], Ling Huang [a, b], Yangjun Wang [a, b], Joost de Gouw [d, e], Li Li [a, b*]**

[a] School of Environmental and Chemical Engineering, Shanghai University, Shanghai, 200444, China

[b] Key Laboratory of Organic Compound Pollution Control Engineering, Shanghai University, Shanghai, 200444, China

[c] Changzhou Institute of Environmental Science, Changzhou, Jiangsu, 213022, China

[d] Cooperative Institute for Research in Environmental Sciences, University of Colorado, Boulder, Colorado, 80309, USA

[e] Department of Chemistry, University of Colorado, Boulder, Colorado, 80309, USA

[f] Tofwerk AG, Thun, Switzerland

[#] These authors contribute equally to this work.

*Correspondence:* Li Li (lily@shu.edu.cn)

## Abstract

The outbreak of COVID-19 promoted strict restrictions to human activities in China, which led to dramatic decrease in most air pollutant concentrations (e.g., $PM_{2.5}$, $PM_{10}$, $NO_x$, $SO_2$, and CO). However, obvious increase of ozone ($O_3$) concentrations was found during the lockdown period in most urban areas of China. In this study, we conducted a field measurement targeting ozone and its key precursors by utilizing a novel proton transfer reaction time-of-flight mass spectrometer (PTR-TOF-MS) in Changzhou, which is representative for the Yangtze River Delta (YRD) city cluster of China. We further applied the integrated methodology including machine learning, observation-based model (OBM), and sensitivity analysis to get insights into the reasons causing the obvious increase of

ozone. Major findings include: (1) By deweathered calculation, we found changes in precursor emissions contributed 1.46 ppbv to the increase in the observed $O_3$ during the Full-lockdown period in 2020, while meteorology constrained 3.0 ppbv of $O_3$ in the Full-lockdown period of 2019. (2) By using an OBM model, we found that although significant reduction of $O_3$ precursors was observed during Full-lockdown period, the photochemical formation of $O_3$ was stronger than that during the Pre-lockdown period. (3) The $NO_x$/VOCs ratio dropped dramatically from 1.84 during Pre-lockdown to 0.79 in Full-lockdown period, which switched $O_3$ formation from VOCs-limited regime to the boundary of $NO_x$- and VOC-limited regime. Additionally, box model results suggested that the decrease in $NO_x$/VOCs ratio during Full-lockdown period could increase the Mean$O_3$ by 2.4 ppbv. Results of this study give insights into the relationship between $O_3$ and its precursors in urban area, and demonstrate reasons causing the obvious increase of $O_3$ in most urban areas of China during the COVID-19 lock-down period. This study also underlines the necessity of controlling anthropogenic OVOCs, alkenes, and aromatics in the sustained campaign of reducing $O_3$ pollution in China.

**Keywords:** Ozone; VOCs; PTR-TOF-MS; COVID-19

# 1. Introduction

At the end of 2019, a tragic coronavirus (COVID-19) occurred, which has caused over 271 million global infection and over 4.51 million deaths as of this writing (12$^{th}$ Feb 2022). To protect people's health, China adopted strict measures to control the spread of this pandemic. Thirty provinces, autonomous regions and municipalities have launched Full-lockdown response (also known as Level I response, roughly from 24$^{th}$ Jan to 25$^{th}$ Feb 2020) as early as 24$^{th}$ Jan 2020 (Shen et al., 2021; Li et al., 2020; Huang et al., 2020). With the effective control of COVID-19 in China, the emergency response level in most provinces (except Hubei province, the hardest-hit region) gradually downgraded to Partial-lockdown (Level II and Level III response, roughly after 25$^{th}$ Feb 2020) (Li et al., 2020), and work resumption started. During Full-lockdown period, all the social events that may cause crowds (excluding transportation and industries that maintained the basic operation of society) were severely restricted. Affected by the pandemic, many factories were shut down, and the on-road traffic volume

and construction activities have been reduced significantly (Zheng et al., 2020). During Full-lockdown period, dramatic decrease of air pollutants (e.g., $PM_{2.5}$, $NO_2$, BC) were found in China, especially in urban areas (Fan et al., 2021; Gao et al., 2021; Li et al., 2020; Xu et al., 2020). Surprisingly, marginal increases of $O_3$ were observed during the lockdown period in YRD region, and this seems to be contradictory to the decrease of most air pollutants (Li et al., 2020). However, as suggested by previous studies, the formation of $O_3$ is significantly influenced by $NO_x$/VOCs ratio and meteorological conditions (temperature, relative humidity and actinic flux) (Zhang et al., 2020a; Zhang et al., 2020b). Therefore, it is essential to investigate the changes of meteorological and emissions conditions to figure out reasons causing the increase of $O_3$ during this pandemic.

Previous studies on the $O_3$ pollution in the YRD region have often focused on the more populated metropolitan areas, such as Shanghai and Nanjing, which are considerably far away from the industrial zones that are essentially responsible for the sources of $O_3$ precursors (Li et al., 2019; Zhang et al., 2020b). Changzhou, located in the center of the Yangtze River Delta (YRD) region, is a typical city with fast urbanization, heavy industrial structure, huge energy consumption, increasing vehicle stocks and frequent air pollution. Therefore, it provides a more representative environment to fully elucidate the mechanism underlying the $O_3$ pollution in the YRD region (Shi et al., 2020). In a companion paper (Jensen et al., 2021), we also demonstrated that Changzhou is representative for the region by analyzing both surface observations and satellite data. According to previous studies, the anthropogenic VOCs emission in Changzhou was around $9\sim12.6\times10^4$ tons/year, among which industries was the dominant source, accounting for 27~47% of the total VOC emissions (Cheng et al., 2016; Fu et al., 2013). It is notable that industrial sources together contributed over 80% of anthropogenic VOC emissions (Sun et al., 2019). Apart from industrial sources, vehicle exhaust accounted for 9%~14% of total VOC emissions (Sun et al., 2019). However, rare observation regarding VOCs characteristics during COVID-19 in Changzhou has been conducted.

Highly time-resolved measurements of VOCs are generally much sparse and could not be easily expanded during the lockdowns. This limits our understanding of how VOCs changed and how the formation of ozone was affected. Here, we used a novel proton transfer reaction time-of-flight mass

spectrometer (PTR-TOF-MS, Tofwerk, Model Vocus Elf, CHE) to conduct online observation of VOCs in Changzhou. The characteristics of VOCs and the variations of general air pollutants in each emergency response period were analyzed. Additionally, ozone formation during each period was investigated by an OBM model. Although terrifying impact has been caused by the COVID-19, it provided a rare experiment to analyze the variations of VOCs and $NO_x$ due to changes of anthropogenic activities in a typical city of China. Furthermore, results of this study offer theoretical support for formulating refined ozone management policy in China.

# 2. Methodology

## 2.1 Field measurement

The field campaign was conducted from 8$^{th}$ Jan to 31$^{st}$ Mar 2020 at a sampling site located on the rooftop of a building at Changzhou Environmental Monitoring Center (CEMC, 31.76° N, 119.96° E), which was approximately 15 m above ground level. As a typical urban monitoring station, this site is in the center of Changzhou city, surrounded by residential and commercial area, which is also adjacent to the main transportation junction in Changzhou (Figure 1). According to local epidemic prevention policies, we roughly classified the measurement periods into three stages: Pre-lockdown (8$^{th}$ January to 23$^{rd}$ January 2020), Full-lockdown (25$^{th}$ January to 24$^{th}$ February 2020), Partial-lockdown (25$^{th}$ February to 28$^{th}$ March 2020) as defined in a study of the Yangtze River Delta (Li Li et al., 2020).

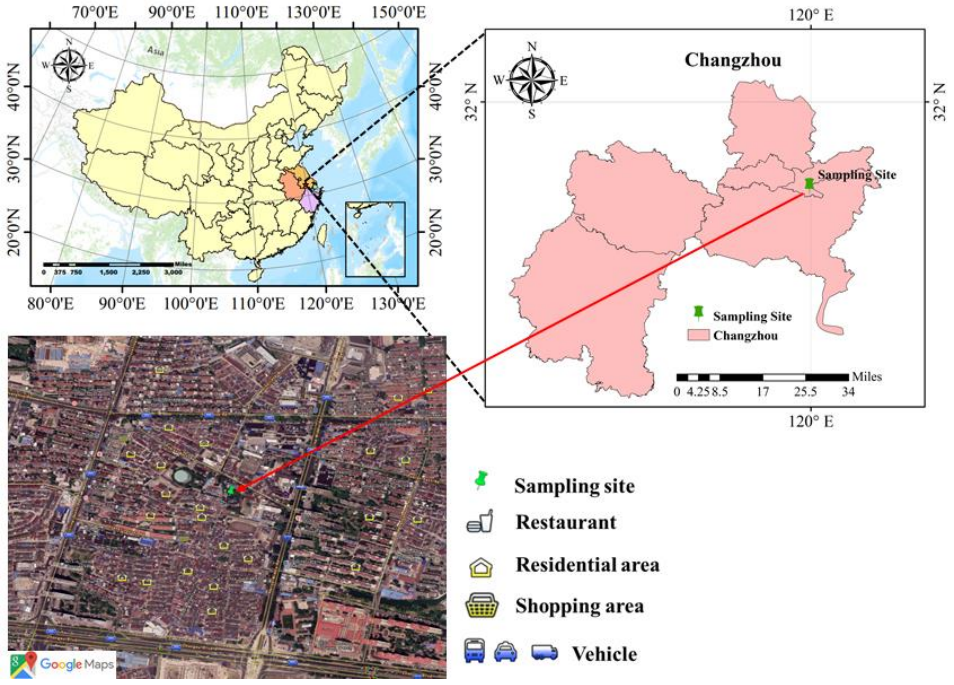


**Figure 1. Location of the sampling site in Changzhou.**

From Jan 8th to Mar 27th, 2020, the concentrations of traditional air pollutants ($PM_{2.5}$, $PM_{10}$, $NO_x$, $SO_2$, CO, $O_3$) as well as meteorological parameters were monitored by a series of analyzers (Table 1**Error! Reference source not found.**). In particular, 87 VOCs species were quantified, 59 of which were identified, by a PTR-TOF-MS with time resolution of 1 min. Detailed measurement techniques and quality assurance and control has been documented in detail in our companion paper (Jensen et al., 2021). Here, we just briefly introduce the measurement. The air samples were directly drawn into a 3 m-long tube connected to the instrument. A priming pump, with flow rate of 4 L/min, was used to reduce the retention time of the gas sample in the tube. To avoid blocking of inlet tube caused by particles, a particulate filter was assembled at the front of the inlet tube. The pressure of the ion source was set as 2 mbar and the temperature of the reaction chamber was set to 90 °C during the observation. VOCs are ionized by reactions with $H_3O^+$ ions from a discharge, and the product ions are detected by a time-of-light mass analyzer (m/Δm FMHW of 950 at m/Q 107). The PTR-TOF-MS can detect most unsaturated hydrocarbons and VOCs with functional groups but cannot detect species with proton affinities lower than that of water, namely alkanes and small alkenes. Eighteen standard gases (including acetonitrile, acetaldehyde, acrolein, acetone, isoprene, butanone, 2-butanone, benzene, 2-

pentanone, ethyl acetate, toluene, methyl isobutyl ketone, styrene, xylene, trimethylbenzene, naphthalene, a-pinene, and 1,3-dichlorobenzene) with concentrations of 1 ppmv were used for the calibration of the PTR-TOF-MS. In addition, a built-in calibration system was used to control the zero and standard gases.

**Table 1 Measurements performed during the field campaign.**

| Species/Parameter | Experimental Technique |
|---|---|
| T, RH, WS, WD and P | 2000WX, Airmax, USA |
| $O_3$ | 400E, API, USA |
| $NO_x$ (NO and $NO_2$) | T200, API, USA |
| $SO_2$ | T100, API, USA |
| CO | T300, API, USA |
| $PM_{2.5}$ | 5030, Thermo Fisher, USA |
| $PM_{10}$ | 5030, Thermo Fisher, USA |
| VOCs | Vocus Elf, Tofwerk, CHE |

## 2.2 Observation-based model

An OBM model coupled with MCM v3.3.1 was utilized to investigate the atmospheric oxidation capability and the radical chemistry. Detailed information about the chemistry mechanism is available on MCM website (http://mcm.leeds.ac.uk/MCM/, last access 8 Jul 2021). More than 5800 chemical species and 17000 reactions are included in this mechanism. The photolysis frequencies (J values) were calculated as a function of solar zenith angle, altitude using lookup tables, calculated using the Tropospheric Ultraviolet and Visible (TUV) model (Wolfe et al., 2016). Dilution mixing within the boundary layer is considered. However, as a 0-D model, vertical or horizonal transport of airmasses are not involved. The observed meteorological parameters (T, RH, P), trace gases (NO, $NO_2$, CO, $SO_2$, and VOCs) were used to constrain the model. Before each simulation, the model was run 3 days as spin-up to reach a stable state. According to the definition of atmospheric oxidation capability (AOC), AOC is quantified by Eq (1) (Geyer et al., 2001).

$$AOC = \sum_{i=1} k_{Y_i-X}[Y_i][X] \quad (1)$$

where $Y_i$ are the primary pollutants (e.g., VOCs, $CH_4$, and CO); $X$ are atmospheric oxidants (OH, $O_3$, $NO_3$); $k_{Yi}$ are the bimolecular rate constants for the reactions of $Y_i$ and $X$. A high value of AOC indicates fast scavenge of primary air pollutants. Additionally, OH reactivity ($k_{OH}$), defined as the reaction rate coefficients multiplied by the concentrations of the reactants with OH, is also widely used as an indicator of AOC. The value of $k_{OH}$ depends on both the abundances and compositions of primary pollutants and can be calculated by Eq (2).

$$k_{OH} = \sum_i k_{OH+X_i} \times [X_i] \quad (2)$$

where $k_{OH+Xi}$ are the reaction rate coefficients of reaction OH+$X_i$; $Xi$ are the concentrations of pollutants (VOC, $NO_2$, CO, OVOC etc.) (Zhu et al., 2020).

## 2.3 Trend Analysis

Mann-Kendall (MK) trend test is a widely used non-parametric test method (Pathakoti et al., 2021; Zhang et al., 2013). It is applicable to all distributions (that is, the data does not need to meet the assumption of normal distribution), but the data should have no serial correlation. If the data has serial correlation, it will have an impact on the significance level (p value). In this study, the MK trend analysis was performed for individual VOC concentrations during Pre-lockdown and Full-lockdown period. By using the "feast" R package, no obvious serial correlation of individual VOC is found. Therefore, the observed VOC data is suitable for MK test. Detailed description and the calculation formula of MK trend test could be found in the study of Pathakoti et al. (2021) and Alhathloul et al. (2021). A positive z value from the MK test indicates increasing trend of the target compound. On the contrary, a negative z value suggests the target compound was decreasing.

Sen's slope, a non-parametric test proposed by Sen (1968), is used in this study to assess the rate of change in individual VOC concentrations. The Sen's slope is selected since it is insensitive to outliers, and does not require a normal distribution of residuals. Sen's slope (Q) is mathematically represented by the following equations.

$$Q = median(SS_{ij}) \quad (3)$$

$$SS_{ij} = \frac{x_j - x_i}{j - i}, 1 \le i \le j \le n \quad (4)$$

where $x_j$ and $x_i$ are concentrations of VOC specie x at time $j$ and $i$ ($1 \le i \le j \le n$), respectively. $SS_{ij}$ is the linear slope between time $i$ and $j$, and Q is the median of $SS_{ij}$. Positive and negative Q values indicate increasing or decreasing trend of VOC specie x, respectively.

## 2.4 Deweathered model

The observed concentrations of $O_3$ could be influenced by meteorological conditions, emissions and/or chemistry. The emissions and chemistry are being treated together and separated from meteorology by the deweathered approach based on the random forest (RF). Hourly data of Unix date (number of seconds since 1970-01-01), Julian day, weekday, hour of day, wind speed (WS), wind direction (WD), temperature (T), relative humidity (RH), and pressure (P), which are available during the whole observation, were used for the deweathered calculation of $O_3$. The missing data was replaced by linear interpolation. Training of the models was conducted on 80% of the input data and the other 20% was withheld from training. To avoid the disadvantage of overfitting during the training of RF, a process called bagging (or bootstrap aggregation) was adopted. Bagging results in new, sampled set called out-of-bag (OOB) data. A decision tree is then grown on the OOB data. Therefore, all the decision trees are grown on different observations and avoid the overfitting (Grange and David (2019)). To determine the value of number of trees (ntree), number of samples (nsample), and the minimal node size, a series of random forests were performed under different choices of ntree, nsample, and minimal node size. The results suggest that the highest coefficient of determination ($R^2$, 0.84) was obtained when ntree, nsample and minimal node size was set as 300, 300, and 5, respectively (Table S1 and S2). More details of this model could be found in the study of Grange and David (2019). The uncertainty of the deweather model is obtained by growing 50 random forest models with the hyperparameters described above, which is the same method as Grange and Carslaw (2019). The mean and standard error of the predicted $O_3$ concentrations is shown in Figure S1, and results of the model are stable during the 50 runs. The differences in observed $O_3$ concentrations ($O_{3,Obs}$) and deweathered $O_3$ concentrations ($O_{3,Normal}$) were regarded as the concentrations contributed

by meteorology ($O_{3,Met}$), which is consistent with the definition in Li et al. (2021). Correspondingly, the differences in $O_{3,Normal}$ concentrations in different periods represent the influence of emissions, since the $O_{3,Normal}$ has already removed the influence of meteorological conditions.

# 3. Results and discussion

## 3.1 Overview of the field campaign

Figure 2 shows the meteorological conditions during the observation. During the whole experiment, the prevailing WD was southeast. The average T and RH was 9.9 ± 5.1℃ and 58.9 ± 17.1%, respectively. Compared to Pre-lockdown period, the concentrations of $PM_{2.5}$, $PM_{10}$, $SO_2$, NO, $NO_2$, TVOC and CO during Full-lockdown period decreased by 48%, 42%, 11%, 65%, 58%, 33% and 39%, respectively. It should be noted that the decreasing ratio of VOC/$NO_x$ is around 1.75, suggesting that the lockdown policy has stronger influence on $NO_x$ emissions than VOC emissions. The $O_3$ concentrations during the same period in 2020 and 2019 are summarized in Table 2. Considering the influence of Chinese New Year, the corresponding period in 2019 was decided according to lunar calendar. It should be noted that, compared to Full-lockdown period in 2019, the mean $O_3$ concentration in 2020 is obviously higher (5.5 ppbv, Figure 2). Meanwhile, the average $O_3$ concentrations in Full-lockdown period in 2020 was 67% higher than that during Pre-lockdown period in 2020. To roughly analyze the cause of the obvious increase of $O_3$ during Full-lockdown period in 2020, we summarized the temperature (T) and relative humidity (RH) in Table 2. The T and RH in Full-lockdown period in 2020 was ~1.6 °C higher and 6.1% lower than that in the same period in 2019, while the P and WS were comparable during the same period in 2020 and 2019 (Table 2). The relatively higher T was in favor of $O_3$ formation during the Full-lockdown period in 2020. As for RH, the influence on $O_3$ is nonlinear (Zhang et al., 2020), and based on our sensitivity test, lower RH could lead to decrease or increase of $O_3$ concentration (Figure S2). Overall, changes in $O_3$ concentrations could be a result of the joint effect of meteorological conditions and emissions/chemistry, the following sections would discuss these influences respectively.

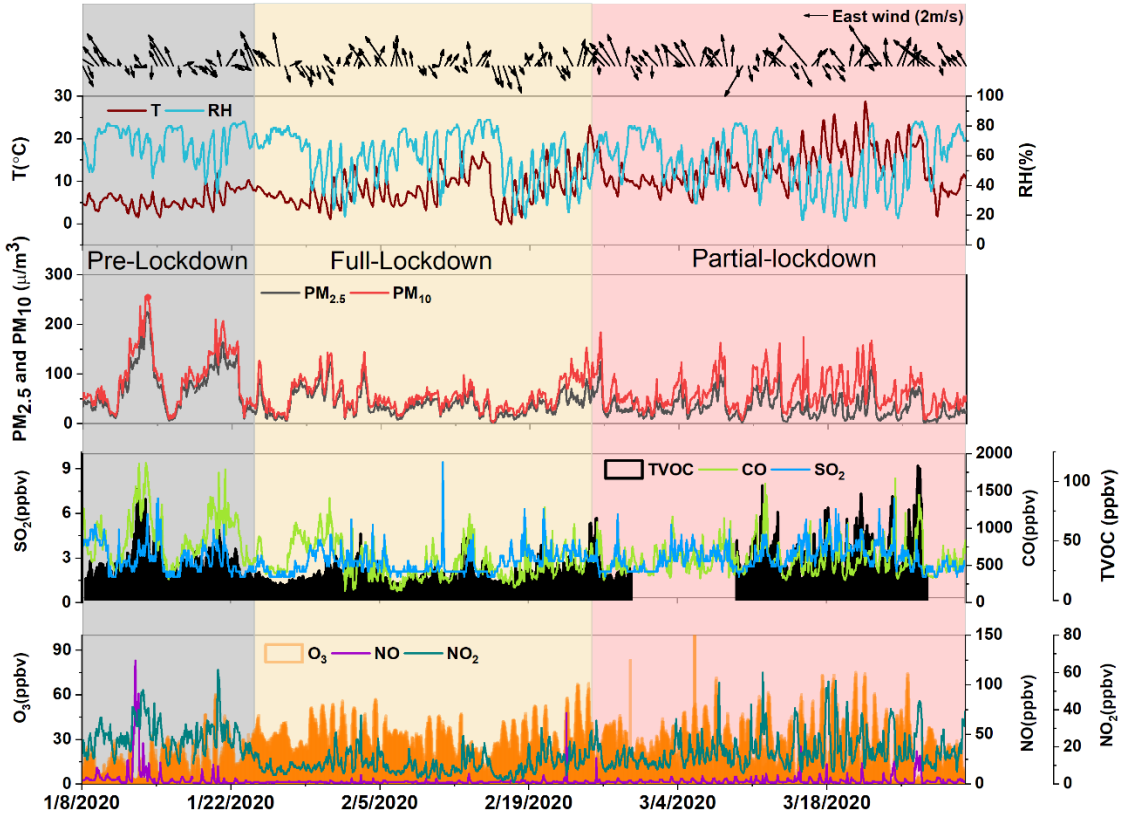


**Figure 2 Time series of meteorological parameters and air pollutants during the whole observation.**

**Table 2 Comparison of average meteorological conditions during Pre-lockdown, Full-lockdown, and Partial-lockdown in 2020 and the same period in 2019.**

| Periods | Date | P (hPa) | RH (%) | T (℃) | Precipitation (mm) | WS (m/s) |
|---|---|---|---|---|---|---|
| Pre-lockdown | (2020.1.8-1.24) | 1025.4 | 84.9 | 4.8 | 0.13 | 1.8 |
| Same period in 2019 | (2019.1.19-2.4) | 1025.6 | 72.7 | 5.2 | 0.05 | 1.9 |
| Full-lockdown | (2020.1.25-2.24) | 1025.6 | 73.0 | 7.3 | 0.09 | 2.1 |
| Same period in 2019 | (2019.2.5-3.7) | 1024.1 | 79.1 | 5.7 | 0.15 | 2.1 |
| Partial-lockdown | (2020.2.25-3.31) | 1018.9 | 69.5 | 12.1 | 0.11 | 2.4 |
| Same period in 2019 | (2019.3.8-4.12) | 1017.6 | 64.0 | 13.8 | 0.02 | 2.0 |

## 3.2 Mechanism affecting the obvious $O_3$ increase

### 3.2.1 Meteorological perspective

Deweathered $O_3$ concentrations were calculated based on the model described in Section 2.4. The difference between $O_{3,Obs}$ and $O_{3,Normal}$ can be regarded as the meteorological influence ($O_{3,Met}$). In

addition, the difference between $O_{3,Normal}$ concentrations in different years could be considered as the influence of emissions ($O_{3,Emi}$). Figure 3 exhibited the average $O_{3,Obs}$, $O_{3,Normal}$, $O_{3,Met}$ during the same periods in 2019 and 2020, respectively. It is obvious that the $O_{3,Obs}$ during Pre-lockdown period is much lower than that during Full-lockdown period in both years, which was partly attributed to negative influence of meteorological condition during Pre-lockdown period (Figure 3). This is consistent with the increasing temperature and solar radiation, which could significantly contribute to the increase in ozone concentration, from Pre-lockdown to Full-lockdown period. It should be noted that meteorology constrained $O_3$ concentrations by 3.9 ppbv during the Full-lock down period in 2019. Apart from the influence of meteorological condition, the $O_{3,Normal}$ in Full-lockdown period in 2020 is still 1.46 ppbv and 0.64 ppb higher than that during Full-lockdown period in 2019 and that during Pre-lockdown period in 2020, indicating that improper decline of precursor emissions was possibly the key reason for the obvious increase of $O_3$ during Full-lockdown period in 2020.

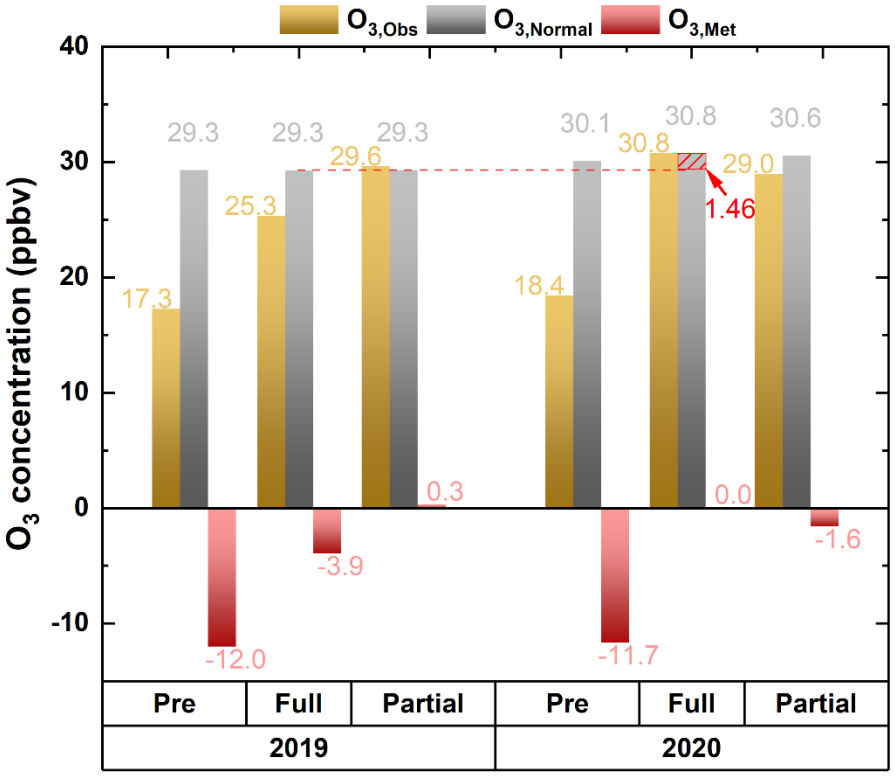


**Figure 3. Comparison of observed (Obs), weather-normalized (Normal), and meteorological-factors-infected**

**(Met) $O_3$ concentrations during the same period in 2019 and 2020.**

### 3.2.2 Ambient VOCs

As mentioned above, the changes in $O_3$ precursor emissions strongly affected the $O_{3,Obs}$, and the changes in VOCs and $NO_x$ emissions would eventually be reflected by the observed concentrations of individual VOCs and $NO_x$. Therefore, the concentrations of each VOC group in different periods were summarized (Figure 4). OVOCs dominated the total VOCs (TVOC) concentrations during the whole observation, with a daily average concentration of 21.44 ± 10.27 ppbv. During Full-lockdown period, the TVOC dropped to 22.19 ±7.9 ppbv from 32.78 ± 13.81 ppbv, which was mainly affected by the decrease in industrial activities and traffic volume. This is proved by the trend of traffic volume, VOCs emission and traffic/industrial-derived VOCs (Text S1 and Figure S3). In addition, Jensen et al. (2021) found the VOC emissions from most industries in Changzhou share the same "U-shape" trend as our study. The most obvious drop was found in aromatics (~54%), followed by OVOCs (~27%), alkenes (~26%), nitrogen hydrocarbon (~25%), and other VOCs (~21%). Additionally, the discrepancy of daytime and nighttime VOCs concentrations during different periods were compared (Figure 4 (A)). The concentration of each VOCs group exhibited higher values during nighttime, which was caused by the low atmospheric oxidation condition and the low atmospheric boundary layer height (Maji et al., 2020; Valach et al., 2015).

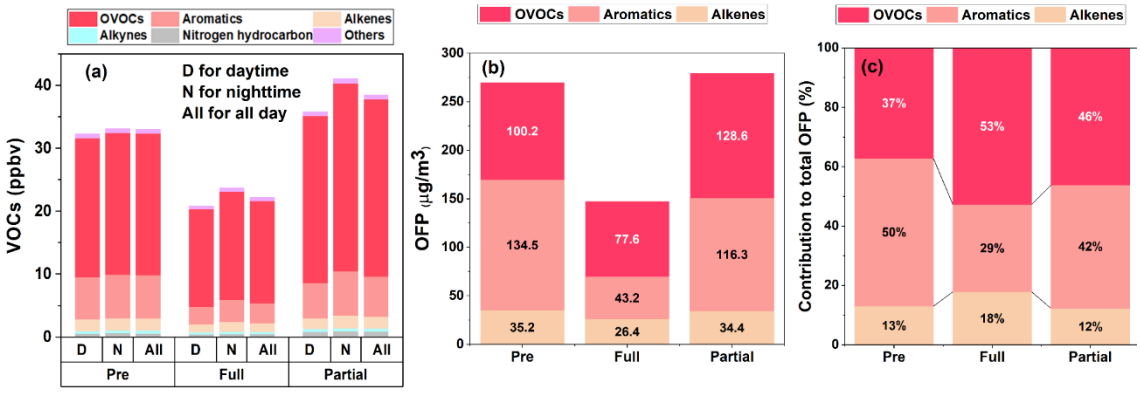


**Figure 4. Comparison of daytime and nighttime VOCs concentrations (A), average OFP (B), and contribution to total OFP (C) during different periods.**

Furthermore, the average concentrations of individual VOCs during different periods were

summarized in Figure 5. Total 42 VOC species exhibited an 'U' shape trend during the whole observation, while formaldehyde (HCHO) and methanol showed an obvious increasing pattern. It should be noted that the measurement of HCHO could be strongly influenced by humidity. Since within the drift tube, the back reaction, which converse the protonated HCHO back into HCHO, is highly humidity dependent (Inomata et al., 2008; Warneke et al., 2011).

To quantitatively evaluate the changes of individual VOC concentrations from Pre-lockdown to Full-lockdown period, when the variations of each VOCs are obvious, we applied MK trend test and Sen's slope analysis based on the hourly average VOCs concentration data (Table S3). Table 3 lists the top 10 VOCs species with decreasing pattern (with negative Q value) from Pre-lockdown to Full-lockdown period. Toluene, benzene and xylene exhibited the most significant decreasing pattern, with a slope of $7.73\times10^{-4}$, $7.36\times10^{-4}$, and $7.20\times10^{-4}$ ppbv $h^{-1}$, respectively. As for $NO_x$ and TVOC, the slope was $-1.62 \times 10^{-2}$ and $5.48\ 10^{-3}$ ppb $h^{-1}$ (Table S3). This result is consistent with the drastic drop of industrial activities and traffic volumes, which are key sources of aromatics and $NO_x$, from Pre-lockdown to Full-lockdown period. Other VOCs, such as ethyl-acetate, acetic acid, acetaldehyde, diethyl sulfide, ethanol, butanol and acrolein are also tightly associated with industrial processes, thereby showed decreasing trend from Pre-lockdown to Full-lockdown period. Additionally, the average diurnal variations of acetonitrile, dimethyl formamide (DMF), and styrene, which are tracers of biomass burning and industrial emission, respectively, exhibited significant reduction during Full-lockdown period (Figure S4), also indicating strong decrease in these emissions. However, formaldehyde and methanol exhibited increasing trend, with a slope of $12.78\times10^{-4}$ and $6.35\times10^{-4}$ ppbv $h^{-1}$, respectively. This could be explained by the secondary formation of HCHO and methanol, which was promoted under better oxidation condition in Full-lockdown period.

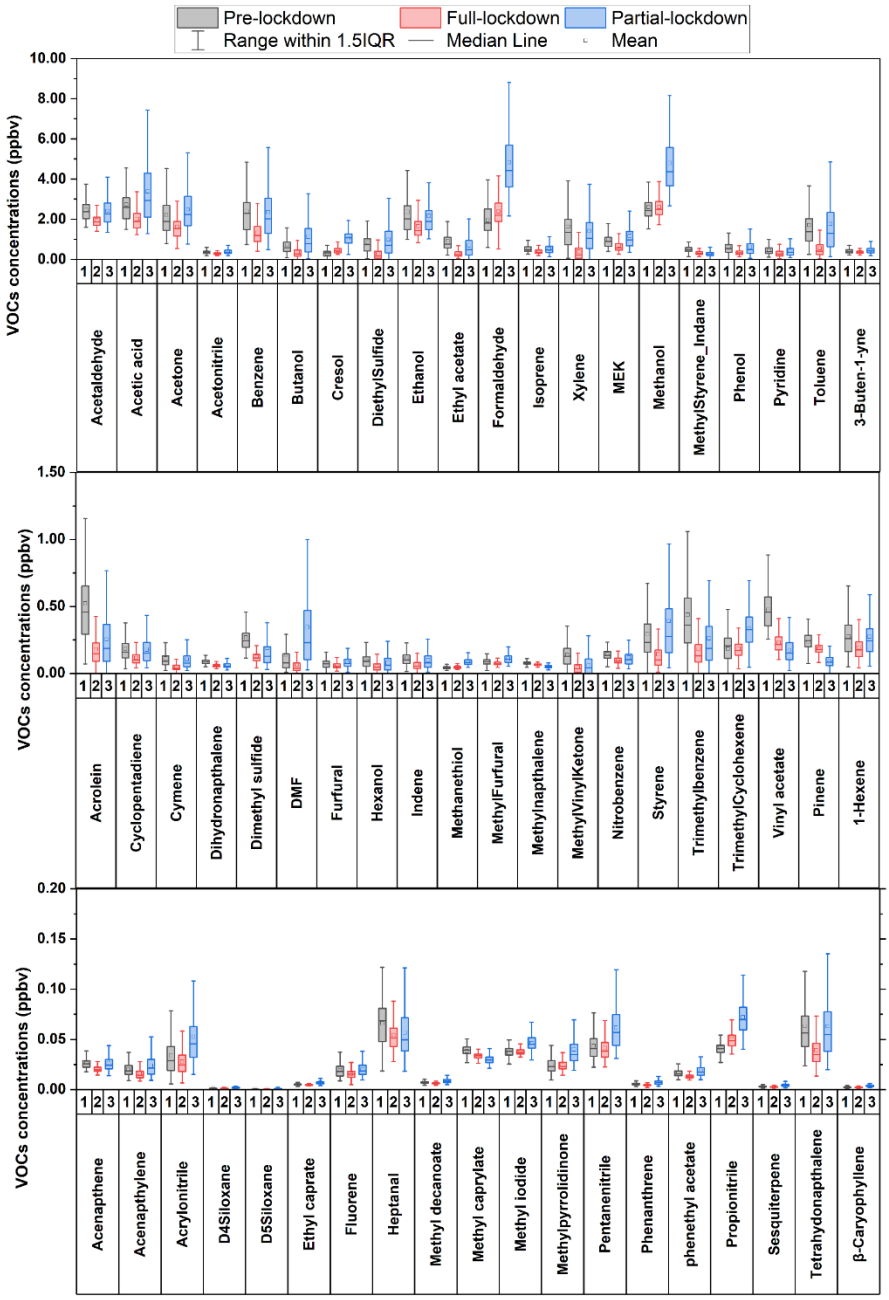


**Figure 5. Concentrations of individual VOC species during different period.**

***MEK, DMF, are abbreviation of Methyl ethyl ketone and dimethylformamide, respectively.**

**Table 3. Top 10 VOCs with decreasing trend from Pre-lockdown to Full-lockdown**

| VOC | Z value | Q *10000 (ppbv $h^{-1}$) | VOC | Z value | Q *10000 (ppbv $h^{-1}$) |
|---|---|---|---|---|---|
| Toluene | -14.02 | -7.73 | Acetaldehyde | -10.31 | -3.95 |
| Benzene | -9.65 | -7.36 | Diethyl sulfide | -9.15 | -3.16 |
| xylene | -12.38 | -7.20 | Ethanol | -5.48 | -3.09 |
| Ethyl-acetate | -18.53 | -5.20 | Butanol | -10.42 | -2.83 |
| Acetic acid | -6.79 | -4.12 | Acrolein | -15.48 | -2.76 |

### 3.2.3 Chemistry perspective

The reactivities of different VOCs vary significantly, hence, ozone formation potential (OFP) is used in this study to assess the potential contribution of active VOCs (including alkenes, aromatics and OVOCs) to $O_3$ formation on the same basis, and it can be calculated by formula (5):

$$OFP_i = MIR_i \times [VOC_i] \quad (5)$$

where $MIR_i$ is the ozone formation potential coefficient for a given VOC species $i$ in the maximum increment reaction of $O_3$, acquired from Carter (2009); $[VOC_i]$ is the concentration of VOC species $i$ (in μg/$m^3$). It should be noted that OFP does not indicate $O_3$ concentration but only serves as a reference for the potential $O_3$ produced via the degradation of VOCs. The time series of total OFP is shown in Figure 6. The average OFP in Pre-lockdown, Full-lockdown, and Partial-lockdown period was 269.4 ± 146.0, 147.2 ± 72.4, 279.3 ± 168.6 μg/$m^3$, respectively. The trend of the total OFP indicates the drastic decrease of VOCs reactivities from Pre-lockdown to Full-lockdown period. During Pre-lockdown period, aromatics were the dominant OFP contributor (49%), followed by OVOCs (38%) and alkenes (13%) (Figure 4). Among VOCs, xylene exhibited the maximum OFP value (68.6 ± 59.3 μg/$m^3$), followed by acetaldehyde (28.8 ± 6.4 μg/$m^3$), toluene (25.7 ± 20.1 μg/$m^3$) trimethylbenzene (25.4 ± 15.8 μg/$m^3$), and formaldehyde (22.7 ± 9.1 μg/$m^3$) (Figure S5). Compared to Pre-lockdown period, the OFP of aromatics decreased dramatically (-91.2 μg/$m^3$) during Full-lockdown period (Figure 4 (B)), which was mainly attributed to the rapid decline of human activities (e.g., transportation and industry). However, the OFP of alkenes and OVOCs only decreased by 8.9 and 22.5 μg/$m^3$, respectively. During the PTR-TOF-MS observation, the most abundant alkenes and aromatics are 1-hexene and isoprene, with the $k_{OH}$ of 100 and 57 $\times 10^{-12}$ $cm^3$ $molecule^{-1}$ $s^{-1}$,

respectively (Atkinson and Arey, 2003). The fast degradation of these alkenes could attribute to the relatively smaller change of OFP from alkenes. As for OVOCs, the secondary formation could compensate the decrease in primary emissions. The OFP values of aromatics and alkenes during Pre-lockdown and Partial-lockdown period are comparable, but OVOCs exhibited higher OFP contribution (~46%) in Partial-lockdown period, which could be attributed to the higher AOC, enhanced solar radiation and temperature during Partial-lockdown period. To compare the average reactivity of VOCs during different periods, we calculated the mean MIR, derived by dividing the total OFP by total VOC concentration, in each period. A higher MIR means stronger capability of VOCs to produce ozone. As shown in Figure 7, the average MIR during Pre-lockdown, Full-lockdown, and Partial-lockdown period was 3.85, 3.53 and 3.68 (g $O_3$/g VOC), respectively. This result suggests that VOC species composition in Full-lockdown is more conductive to ozone formation than that in Pre-lockdown, and Partial-lockdown period. However, the formation of $O_3$ was sensitive to the ratio of $NO_x$/VOCs and meteorological conditions, which can be significantly different in each period. As shown in Figure 7, the average $NO_x$/VOCs ratio in the three periods (shown in) was 1.84, 0.79, and 0.84, respectively, suggesting more $NO_x$ was reduced than VOCs during Full-lockdown period, which could further influence the sensitivity of $O_3$ formation.

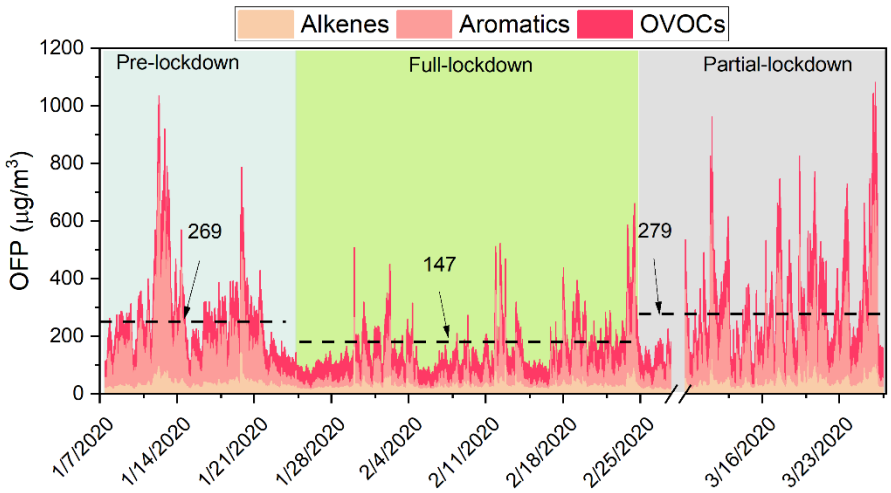


**Figure 6. Time series of OFP during the whole observation period (dash lines represent the average OFP value during each period)**

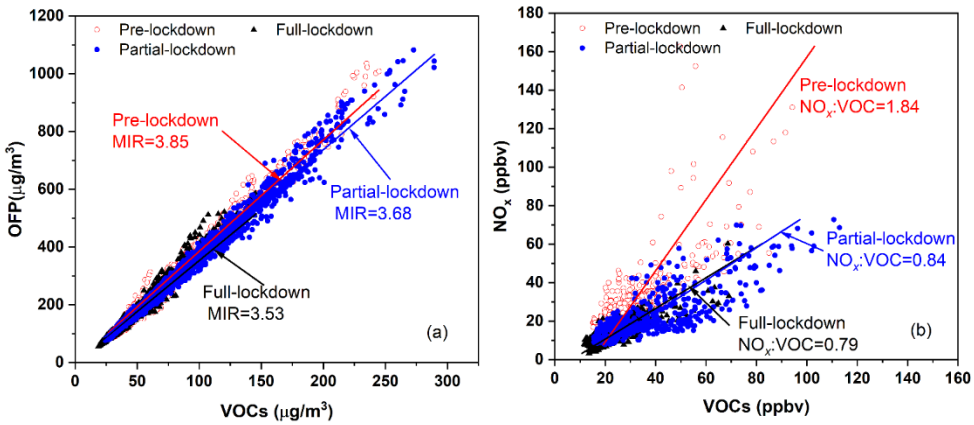


**Figure 7. Plot of 1-hour averaged MIR and NO*x* vs VOCs during three periods.**

To investigate the detailed formation mechanism of $O_3$ in each period, three cases (January 19$^{th}$, February 1$^{st}$, March 14$^{th}$) with stagnant meteorological conditions were chosen. The index of agreement (IOA) of $O_3$ is 0.80, indicating that the model can capture the daytime variation of $O_3$. The simulated daytime OH concentrations exhibited an increasing trend from January 19$^{th}$ to March 14$^{th}$, with an average value of 0.36 ± 0.27 × $10^6$, 0.75 ± 0.54 × $10^6$ and 1.18 ± 0.78 × $10^6$ molecules $cm^{-3}$, respectively. This could be attributed to the increasing solar radiation and temperature from January to March. To analyze the atmospheric oxidation, we calculated the AOC according to Eq(1). The average daytime AOC on Jan 19$^{th}$, Feb 1$^{st}$, and Mar 14$^{th}$ was 0.26 ± 0.35, 0.23 ± 0.33, and 0.31 ± 0.38 molecules $cm^{-3}$ $s^{-1}$, respectively (Figure 9). Comparatively, these values are much lower than those simulated for Shanghai and Beijing (Liu et al., 2012; Zhu et al., 2020; Zhang et al., 2021) in summer, mainly due to the meteorological conditions in winter season. It is notable that the simulated OH on Jan 19$^{th}$ was significantly lower than that on Feb 1$^{st}$, but the AOC on Jan 19$^{th}$ was comparable to that on Feb 1$^{st}$. This should be ascribed to the abundant primary pollutants, which efficiently react with OH, during Pre-lockdown period.

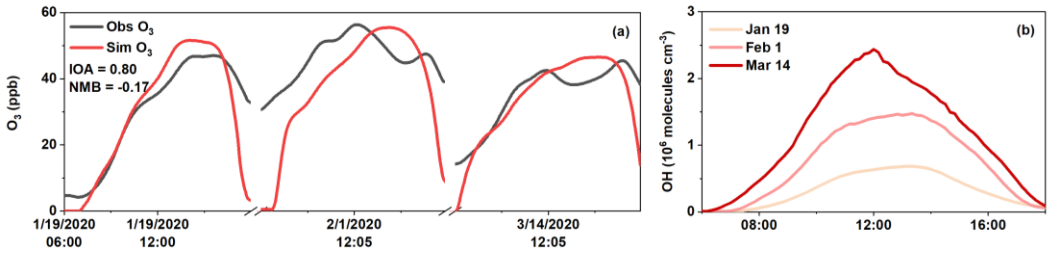


**Figure 8. Comparison of simulated and observed $O_3$ (a) and simulated daytime OH concentrations (b) in three cases.**

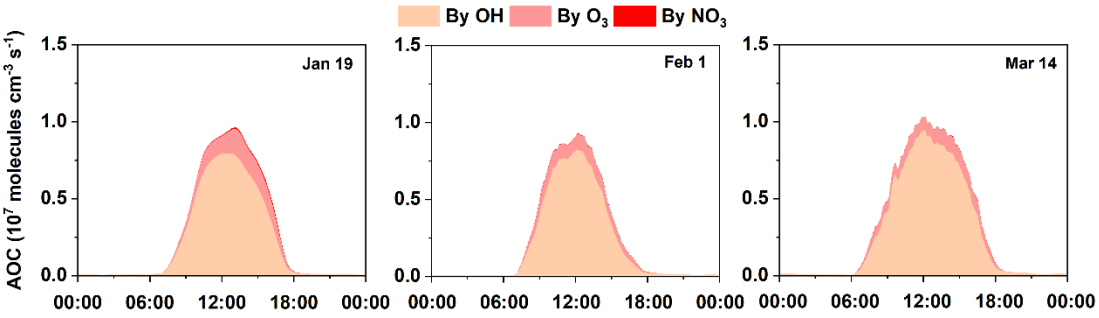


**Figure 9. Diurnal variation of AOC in three cases**

The daytime variations of OH reactivity calculated by OBM model are exhibited in Figure 10, including the contribution from measured pollutants (e.g., VOCs, $NO_x$, and CO) and model-simulated species (OVOCs). Generally, the $k_{OH}$ assessed at Changzhou was in the range of 9~32 $s^{-1}$, which was comparable to that calculated for other cities in China (e.g., Shanghai 4.6~25 $s^{-1}$, Zhu et al., 2020, Chongqing 15~25 $s^{-1}$, Tan et al., 2019 and Beijing 15~25 $s^{-1}$, Tan et al., 2019). It is obvious that OH reactivity peaked in the morning, with maximum values of 31.76, 17.98, and 17.30 $s^{-1}$, respectively. The OH reactivity from $NO_2$ exhibited obvious daytime variation, especially during the morning rush hour, which lead to the peak $k_{OH}$ value during morning. The OH reactivity ($k_{OH}$) on Feb 1$^{st}$ was much lower than that in the other two cases, which was mainly due to the abundance of emissions during Pre-lockdown and Partial-lockdown period. Compared to Jan 19$^{th}$, the $k_{OH}$ from $NO_2$ on Feb 1$^{st}$ and Mar 14$^{th}$ showed lower levels, with an average value of 2.62 and 3.35 $s^{-1}$, respectively. This corresponds with the dramatic drop of traffic volume during lockdown periods. Similarly, compared to Jan 19$^{th}$, the $k_{OH}$ from alkenes and aromatics were lower on Feb 1$^{st}$ and Mar 14$^{th}$. As $k_{OH}$ from OVOC,

it shared same trend as OVOC concentration, which reached the minimum value (5.56 $s^{-1}$) during the Full-lockdown period.

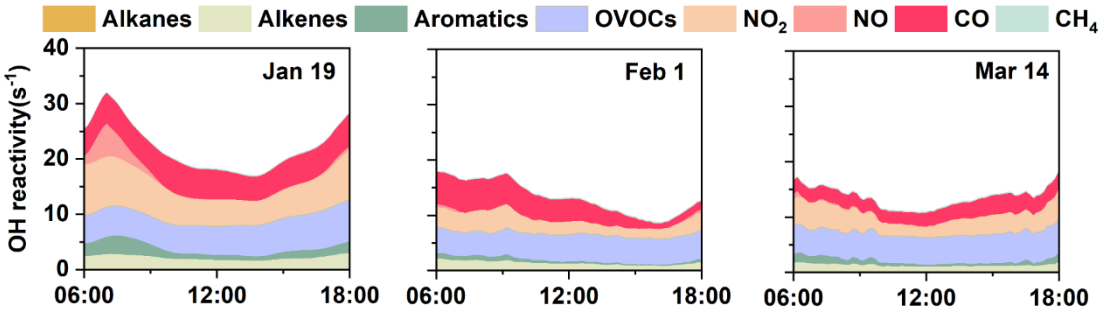


**Figure 10. Daytime variation of OH reactivity in three cases**

To investigate the variation of $O_3$ during different periods, the formation and loss pathways of $O_3$ were calculated (Figure 11). The formation of $O_3$ ($P(O_3)$) was dominated by $HO_2$+NO and $RO_2$+NO pathways. Although the average MIR during Full-lockdown period was the minimum among the three periods, the $P(O_3)$ on Feb 1st was higher than that on Jan 19th. This could be attributed to the higher AOC and better photochemical conditions during Full-lockdown period. Similarly, much higher $P(O_3)$ was found on March 14th. To avoid the influence of meteorological conditions and test the potential mean $O_3$ (Mean$O_3$) concentrations under different $NO_x$/VOCs ratios, a series of scenario analyses were performed based on the average condition during the whole observation, and the isopleths of Mean$O_3$ concentrations are exhibited in Figure. 12. Note that the value of temperature and photolysis frequencies (J values) in the scenario analyses could be higher than the actual value during Pre-lockdown period and could further lead to overestimation of simulated Mean$O_3$ during Per-lockdown period. Additionally, the VOCs concentrations mentioned in this section only represent the VOC species in the MCM mechanism. By connecting the inflection points in each $O_3$ isopleth, we get the ridge line, which divides the whole regime into $NO_x$-sensitive and VOCs-sensitive regimes (Figure. 12). During Pre-lockdown period, the $O_3$ formation was in VOC-limited regime (triangles in Figure. 12), with an average $NO_x$/VOC ratio of 1.84. As for Full-lockdown period, significant decrease of NO*x* and VOC emissions was observed, and the $NO_x$/VOCs ratio dropped to 0.79, which gradually switched the $O_3$ formation to the junction of VOCs-limited and $NO_x$-limited regimes, especially on Feb 16th and Feb 17th (circles in the red rectangle in Figure. 12), when the $O_3$ formation went into

$NO_x$-limited regime. During Partial-lockdown period, increasing of VOCs and $NO_x$ emission again dragged the formation of $O_3$ back into VOCs-limited regime (triangles in Figure. 12). Interestingly, although a great deal of $NO_x$ and VOCs emissions were diminished during Full-lockdown period, the average Mean$O_3$ in Full-lockdown was supposed to be 2.4 ppbv higher than that in Pre-lockdown period. This result is consistent with the trend of the observed MDA8 $O_3$ and the results of the deweathered calculation. Therefore, expect for the influence of meteorology, the improper $NO_x$/VOCs reduction ratio and further influence on chemistry was the key reason for the obvious increase of $O_3$ during Full-lockdown period in Changzhou in 2020.

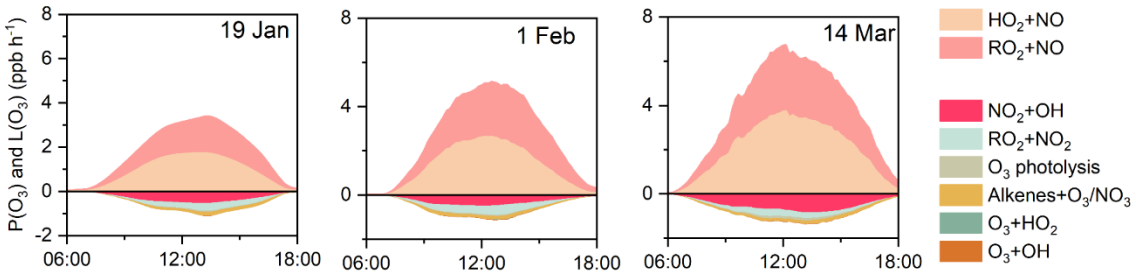


**Figure 11. Daytime variation of P($O_3$) and L($O_3$) in three cases**

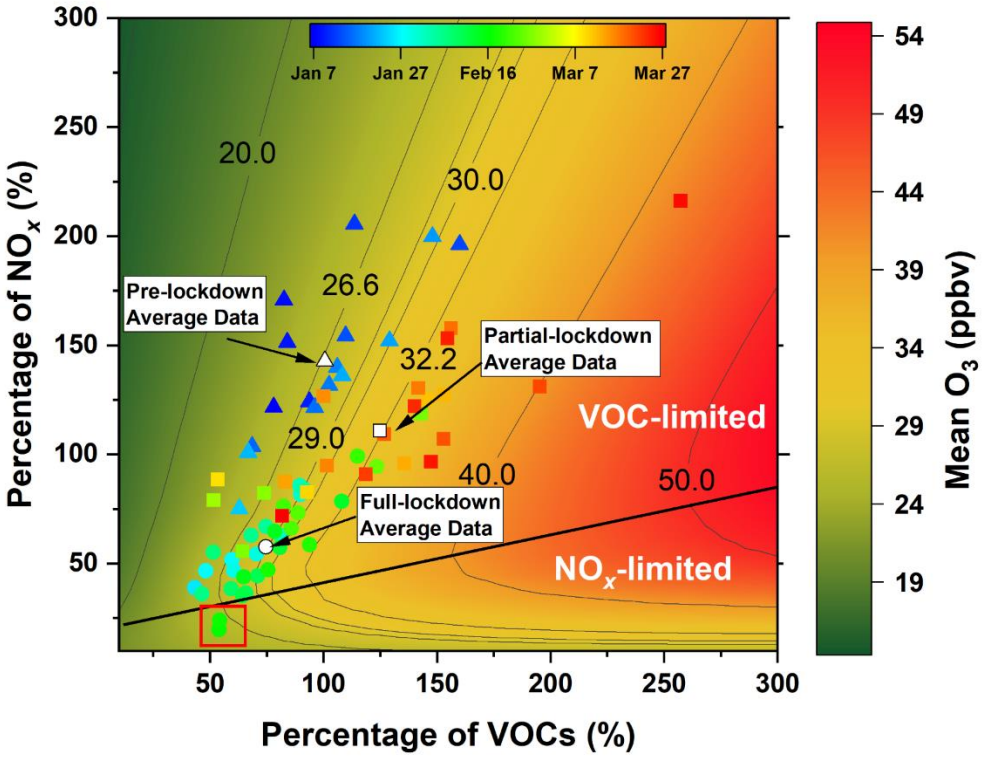

**Figure. 12 Mean$O_3$ isopleth. The colored circles, triangles, and rectangles represent the daily average concentrations of $NO_x$ and VOCs during Pre lockdown, Full-lockdown, and Partial-lockdown period, respectively. The white circle, triangle, and rectangle indicates the average $NO_x$ and VOCs concentrations during Pre lockdown, Full-lockdown, and Partial-lockdown period, respectively.**

The scenario analyses raise a question: how much $O_3$ would change as a function of reduction of $NO_x$ and VOCs? Therefore, the reduction percentage of $O_3$ ($\Delta O_3/O_3$) during Pre-lockdown period as a function of reduction of VOCs and NO*x* were calculated, and the result could be regarded as a potential to control $O_3$ pollution. Based on the VOCs species in MCM v3.3.1, we classified the measured VOCs into four groups: alkenes (n-butene); aromatics (including benzene, toluene, phenol, xylene, styrene, cresol, and trimethylbenzene); OVOCs (including methanol, ethanol, formaldehyde, aldehyde, acrolein, methyl vinyl ketone, methyl ethyl ketone, ethyl acetate, methyl isobutyl ketone, hexanol, and heptanal); and BVOCs (isoprene, pinene, and caryophyllene). The results in Figure 13(a) indicate that more reduction potential of $O_3$ could be achieved by diminishing aromatics, followed by BVOCs, OVOCs, and alkenes. It should be noted that many light alkanes and active alkenes, such as ethene and propene, could not be measured by the PTR-TOF-MS and might further lead to the underestimation of ozone production from alkanes and alkenes. Additionally, this comparison has a drawback of being influenced by the concentrations of VOCs. To normalize the influence of concentrations of VOCs, the descent rate of $O_3$ ($\Delta O_3$ (ppbv)/ $\Delta$VOCs (ppbv)) as a function of reduction percentage of VOCs were calculated (Figure 13 (b)). $O_3$ exhibited the highest dependence on BVOCs, with an average descent rate of 3.74 ± 0.09 ppbv/ppbv. Differing from the result in Figure 13 (a), diminishing alkenes could lead to decrease of $O_3$ by an average declining rate of 1.69 ± 0.01 ppbv/ppbv. On the contrary, reduction of $NO_x$ would lead to increase of $O_3$, with an average rate of 1.29 ± 0.21 ppbv/ppbv (Figure S6). Although the descent rate of $O_3$ turned to decrease and the sensitivity of $O_3$ formation get into NO*x*-limited regime when over 70% of $NO_x$ were eliminated, it still causes net increase of $O_3$.

Although diminishing BVOCs seems to the most efficient way to restrain $O_3$ pollution, most of BVOCs were emitted directly from plants and could not be easily controlled. Besides, huge number of

OVOCs (such as formaldehyde, aldehyde, methanol, ethanol, methyl vinyl ketone, methyl ethyl ketone, etc.) could be directly emitted from anthropogenic processes or secondary generated from the oxidation of precursors (such as alkenes and aromatics), which complicates the control of OVOCs. Therefore, considering the reduction potential and descent rate of $O_3$, more efforts are needed on the control of alkenes and aromatics.

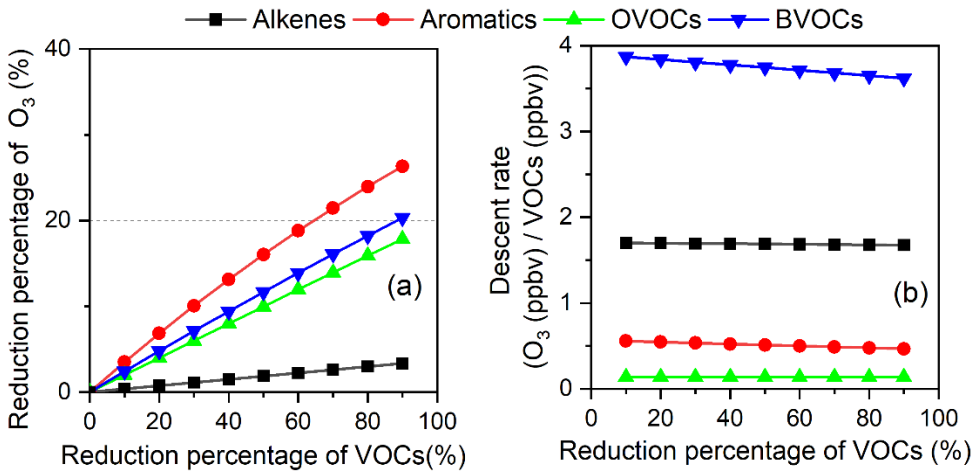


**Figure 13. Reduction percentage of $O_3$ as a function of reduction percentage of VOCs (a); descent rate of $O_3$ as a function of reduction percentage of VOCs (b).**

## 3.3 Uncertainty analysis

Due to limitations in the observations, several issues should be noted in the application of the OBM model to evaluate the local chemistry in the present study. Firstly, deficiency of the observation of C2~C5 alkenes and alkanes could lead to underestimation of the simulated $O_3$. We can only obtain the C2~C5 alkenes and alkanes concentrations from the observation during the autumn of 2018 at the same site. To analyze the uncertainties from this disadvantage, we have done simulation by including assumed diurnal variation of ethene, propene, butene, ethane, propane and butane which are key C2~C5 alkenes and alkanes at this site, in the model. On average, adding 0.5~2 times alkenes or alkanes could lead to 1.65%~9.49% or 1.37~5.36% increase of simulated $O_3$, respectively (Figure S7 and S8). In addition, the deficiency of C2~C5 has potential to cause uncertainty in $O_3$ formation potential. To quantify this impact, the EKMA analysis with the hypothetical diurnal variation of C2~C5 was also performed. Generally, adding C2~C5 alkenes and alkanes in the model would lead to

slight increase of the simulated $O_3$, and could not obviously change the shape of $O_3$ isopleth (Figure S9). Therefore, the influence of the deficiency of C2~C5 alkenes and alkanes on the $O_3$ formation sensitivity is negligible. It should be noted that, this sensitivity analysis is based on the "hypothetical" diurnal variation of C2~C5 alkenes and alkanes, which would bring in uncertainty. We hope a wider range of VOCs would be monitored simultaneously in future field campaign and avoid this deficiency. Secondly, the photolysis frequencies (J values) were calculated as a function of solar zenith angle, altitude using lookup tables, calculated using the Tropospheric Ultraviolet and Visible (TUV) model, which could lead to uncertainty in the simulation of $O_3$. Hence, we analysis the influence of J values by increasing or decreasing the photolysis rates by 10% and 20%. Results showed that the simulated $O_3$ could decrease or increase by 25.14% or 21.73%, respectively, when photolysis rates were decreased or increased by 20% (Figure S10). In addition, the J values, which directly or indirectly influence the recycling of $RO_x$, could lead to uncertainty in the calculation of AOC and $k_{OH}$. Based on above sensitivity analysis, we found the relative changes in AOC and $k_{OH}$ by 1% changes in J values was 1.07% and 0.14%, respectively. Therefore, the J values is recommended to be measured during future observations.

## 4. Conclusions

After the outbreak of COVID-19, strict epidemic prevention measures have been adopted throughout China, leading to dramatic decrease in traffic volume and industrial activities. Affected by the decrease of number of vehicles on the road, non-essential industrial productivity, and associated pollutant emissions, most of the air pollutants (e.g., $PM_{2.5}$, $PM_{10}$, NO, $NO_2$, $SO_2$, and VOCs) dropped to a lower level during lockdown period (especially during Full-lockdown period). However, $O_3$ increased compared to that during the same period in 2019 in many urban areas of China. To figure out the reasons for this obvious increase of $O_3$, the characteristics of $O_3$ precursors ($NO_x$, VOCs) during Pre-lockdown, Full-lockdown, and Partial-lockdown periods in Changzhou were analyzed. Although this study was conducted in single city of China, the representativeness of Changzhou guaranteed the applicability of the results the YRD region. Results suggested that the decrease of

human activities during Full-lockdown period significantly suppressed the emissions of $NO_x$ and VOCs, which further lead to dramatic drop in the concentrations of most VOCs, especially aromatics. As a result, the NO*x*/VOCs ratios dropped from 1.84 at Pre-lockdown period to 0.79 during Full-lockdown period. By deweathered calculation, we found that meteorology constrained $O_3$ concentration by 3.9 ppbv during Full-lockdown period in 2019, but exhibited negligible influence on that during the same period in 2020. However, compared to Full-lockdown period in 2019, changes in precursor emissions led to 1.46 ppbv increase in $O_3$ concentrations during the same period in 2020. To verify this result, a box model was used to simulate the formation of $O_3$. Results show that the AOC level during Full-lockdown was comparable to that during Pre-lockdown period, but the formation rate of $O_3$ was much higher during Full-lockdown period. By scenario analysis, we found the decrease of $NO_x$ and VOCs in Full-lockdown period dragged the formation of $O_3$ from VOC-sensitive regime to the junction of VOCs- and $NO_x$-limited regime, and the average simulated Mean$O_3$ in Full lockdown period could be 2.4 ppbv higher than that in Pre-lockdown period. Although the deweathered model and OBM model shows differences in the emission-derived change of $O_3$, the results together point out that the improper reduction of $NO_x$ and VOCs was the key reason for the obvious increase of $O_3$ during Full-lockdown period in 2020. Overall, the outbreak of COVID-19 has caused devastation over the world. However, it provided an extreme experiment to investigate the $O_3$ formation under strict emission control policies and provided insights into the policy formulation for diminishing $O_3$ pollution in the YRD region. The data indicate that the concentrations of VOCs and $NO_x$ have changed dramatically during the pandemic, a common situation also found in other Chinese cities, and led to the switch of $O_3$ formation sensitivity. These results have a clear indication that, in the future, more efforts should be paid on the reduction ratio of anthropogenic VOCs and NO*x*.

## Acknowledgement

This study was financially sponsored by the National Natural Science Foundation of China (grant 42075144, 41875161, 42005112), and the Shanghai Sail Program (no. 19YF1415600).

# References


Alhathloul, SH., Khan, AA., Mishra, AK.. Trend analysis and change point detection of annual and seasonal horizontal visibility trends in Saudi Arabia. Theoretical and Applied Climatology 2021; 144: 127-146.

Atkinson, R. and Arey, J.: Atmospheric Degradation of Volatile Organic Compounds, Chemical Reviews 2003; 103, 4605–4638.

Jensen, A., Liu, ZQ., Tan, W., Dix, B., Chen, TS., Koss, A., Zhu, L., Li, Li., Gouw, J. Measurements of Volatile Organic Compounds during the COVID-19 Lockdown in Changzhou, China. Geophysical Research Letters 2021.

Carter, W. Updated maximum incremental reactivity scale and hydrocarbon bin reactivities for regulatory applications. California Air Resources Board Contract 2009; 339.

Cheng, Z., Zhang, J., Zhou, J., Sun, J., Zhou, W., Chen, C., Zheng, J., Wang, TJ. Air pollutant emission inventory and distribution characteristics in Changzhou (in Chinese). The Administration and Technique of Environmental Monitoring 2016; 28: 24-28.

Fan, L., Fu, S., Wang, X., Fu, Q., Jia, H., Xu, H., Cheng, J. Spatiotemporal variations of ambient air pollutants and meteorological influences over typical urban agglomerations in China during the COVID-19 lockdown. Journal of Environmental Sciences (China) 2021; 106: 26-38.

Fu, X., Wang, S., Zhao, B., Xing, J., Cheng, Z., Liu, H., Hao, J. Emission inventory of primary pollutants and chemical speciation in 2010 for the Yangtze River Delta region, China. Atmospheric Environment 2013; 70: 39-50.

Gao, C., Li, S., Liu, M., Zhang, F., Achal, V., Tu, Y., Zhang, S., Cai, C. Impact of the COVID-19 pandemic on air pollution in Chinese megacities from the perspective of traffic volume and meteorological factors. Science of The Total Environment 2021; 773: 145545.

Geyer, A., Alicke, B., Konrad, S., Schmitz, T., Stutz, J., and Platt, U. Chemistry and oxidation capacity of the nitrate radical in the continental boundary layer near Berlin, Journal of Geophysics Research 2001; 106, 8013–8025.

Huang, L., Liu, Z., Li, H., Wang, Y., Li, Y., Zhu, Y., Ooi, M., An, J., Shang, Y., Zhang, D., Chan., A., Li, L. The Silver Lining of COVID-19: Estimation of short-term health impacts due to lockdown in the Yangtze

River Delta Region, China. GeoHealth 2020; 4: e2020GH000272.

Inomata, S, Tanimoto, H, Kameyama, S., Tsunogai, U., Irie, H., Kanaya, Y., Wang, Z. J. A. C., and Physics: Determination of formaldehyde mixing ratios in air with PTR-MS: laboratory experiments and field measurements, 8, 273-284, 2008.

Li, L., An, J., Huang, L., Yan, R., Huang, C., and Yarwood, G. Ozone source apportionment over the Yangtze River Delta region, China: Investigation of regional transport, sectoral contributions and seasonal differences, Atmospheric Environmental 2019; 202, 269–280.

Li, L., Li, Q., Huang, L., Wang, Q., Zhu, A., Xu, J., et al. Air quality changes during the COVID-19 lockdown over the Yangtze River Delta Region: An insight into the impact of human activity pattern changes on air pollution variation. Science of the Total Environment 2020; 732:139282.

Li, R., Zhao, Y., Fu, H., Chen, J., Peng, M., and Wang, C.: Substantial changes in gaseous pollutants and chemical compositions in fine particles in the North China Plain during the COVID-19 lockdown period: Anthropogenic vs. meteorological influences, 21, 8677–8692, https://doi.org/10/gkgxw6, 2021.

Liu, Z., Wang, Y., Gu, D., Zhao, C., Huey, LG., Stickel, R., et al. Summertime photochemistry during CAREBeijing-2007: RO*x* budgets and $O_3$ formation. Atmospheric Chemistry and Physics 2012; 12: 7737-7752.

Maji, S., Beig, G., Yadav, R. Winter VOCs and OVOCs measured with PTR-MS at an urban site of India: Role of emissions, meteorology and photochemical sources. Environmental Pollution 2020; 258: 113651.

Pathakoti, M., Santhoshi, T., Aarathi, M., Mahalakshmi, DV., Kanchana, AL., Srinivasulu, J., et al. Assessment of Spatio-temporal Climatological trends of ozone over the Indian region using Machine Learning. Spatial Statistics 2021; 43: 100513.

Sen, PK. Estimates of the regression coefficient based on Kendall's tau. Journal of the American statistical association 1968; 63: 1379-1389.

Shen, L., Zhao, T., Wang, H., Liu, J., Bai, Y., Kong, S., et al. Importance of meteorology in air pollution events during the city lockdown for COVID-19 in Hubei Province, Central China. Science of the Total Environment 2021; 754, 142227.

Shi, X., Ge, Y., Zheng, J., Ma, Y., Ren, X., and Zhang, Y. Budget of nitrous acid and its impacts on atmospheric oxidative capacity at an urban site in the central Yangtze River Delta region of China,

542 Atmospheric Environment 2020; 238.
543 Sun, K., Zhou, J., Ding, H., Chen, X., Liu, Z., Xue, P. Anthropogenic source VOCs emission inventory of
544 Changzhou city (in Chinese). Environmental Monitoring and Forewarning 2019; 11: 57-62.
545 Tan, Z., Lu, K., Jiang, M., Su, R., Wang, H., Lou, SR., et al. Daytime atmospheric oxidation capacity in
546 four Chinese megacities during the photochemically polluted season: a case study based on box model
547 simulation. Atmospheric Chemistry and Physics 2019; 19: 3493-3513.
548 Valach, AC., Langford, B., Nemitz, E., Mackenzie, AR., Hewitt, CN. Seasonal and diurnal trends in
549 concentrations and fluxes of volatile organic compounds in central London. Atmospheric Chemistry and
550 Physics 2015; 15: 7777-7796.
551 Venter, ZS., Aunan, K., Chowdhury, S., Lelieveld, J. COVID-19 lockdowns cause global air pollution
552 declines. Proceedings of the National Academy of Sciences of the United States of America 2020; 117:
553 18984-18990.
554 Wang, W., Li, X., Shao, M., Hu, M., Tan, T. The impact of aerosols on photolysis frequencies and ozone
555 production in Beijing during the 4-year period 2012–2015. Atmos. Chem. Phys. 19, 9413-9429 (2019).
556 Wang, W., Parrish, D., Li, X., Shao, M., Zhang, Y. Exploring the drivers of the increased ozone production
557 in Beijing in summertime during 2005–2016. Atmos. Chem. and Phys. 20, 15617-15633 (2020).
558 Warneke, C., Veres, P., Holloway, J., Stutz, J., Tsai, C., Alvarez, S., Rappenglueck, B., Fehsenfeld, F., Graus,
559 M., and Gilman, J. J. A. M. T.: Airborne formaldehyde measurements using PTR-MS: calibration,
560 humidity dependence, inter-comparison and initial results, 4, 2345-2358, 2011.
561 Wolfe, GM., Marvin, MR., Roberts, SJ., Travis KR, Liao J. The Framework for 0-D Atmospheric Modeling
562 (F0AM) v3.1. Geoscientific Model Development 2016; 9: 3309-3319.
563 Xu, L., Zhang, J., Sun, X., Xu, S., Shan, M., Yuan, Q., et al. Variation in concentration and sources of black
564 carbon in a megacity of China during the COVID-19 pandemic. Geophysical Research Letters 2020; 47:
565 e2020GL090444.
566 Zhang, D., Cong, Z., Ni, G. Comparison of three Mann-Kendall methods based on the China's
567 meteorological data. Advances in Water Science 2013; 24: 490-496.
568 Zhang, K., Huang, L., Li, Q., Huo, J., Duan, Y., Wang, Y., Yaluk, E., Wang, Y., Fu, Q., and Li, L.: Explicit
569 modeling of isoprene chemical processing in polluted air masses in suburban areas of the Yangtze River

570 Delta region: radical cycling and formation of ozone and formaldehyde, Atmos. Chem. Phys., 21, 5905-
571 5917, 10.5194/acp-21-5905-2021, 2021.
572 Zhang, K., Li, L., Huang, L., Wang, Y., Huo, J., Duan, Y., et al. The impact of volatile organic compounds
573 on ozone formation in the suburban area of Shanghai. Atmospheric Environment 2020a; 232: 117511.
574 Zhang, K., Xu, J., Huang, Q., Zhou, L., Fu, Q., Duan, Y., et al. Precursors and potential sources of ground-
575 level ozone in suburban Shanghai. Frontiers of Environmental Science and Engineering 2020b; 14: 1-12.
576 Zhang, P., Chen, T., Liu, J., Chu, B., Ma, Q., Ma, J., and He, H.: Impacts of Mixed Gaseous and Particulate
577 Pollutants on Secondary Particle Formation during Ozonolysis of Butyl Vinyl Ether, 54, 3909–3919,
578 https://doi.org/10/gpd9p2, 2020.
579 Zheng, H., Kong, S., Chen, N., Yan, Y., Liu, D., Zhu, B., et al. Significant changes in the chemical
580 compositions and sources of PM2.5 Wuhan since the city lockdown as COVID-19. Science of the Total
581 Environment 2020; 739: 140000.
582 Zhu, J., Wang, S., Wang, H., Jing, S., Lou, S., Saiz-Lopez, A., et al. Observationally constrained modeling
583 of atmospheric oxidation capacity and photochemical reactivity in Shanghai, China. Atmospheric
584 Chemistry and Physics 2020; 20: 1217-1232.
585